Crosstalk between immune and programmed cell death and their application in colorectal cancer risk stratification

CHAOQUN WU[1], YUESHUANG CAI[2], SHAO CHEN[2], YUELIAN HUANG[2] and QIUMEI WU[3]

[1]General Surgery Department 2, Central People's Hospital of Zhanjiang, Zhanjiang, Guangdong 524000, P.R. China;
[2]Endoscope Treatment Department, Central People's Hospital of Zhanjiang, Zhanjiang, Guangdong 524000, P.R. China;
[3]Oncology Department 1, Central People's Hospital of Zhanjiang, Zhanjiang, Guangdong 524000, P.R. China

Received June 1, 2025; Accepted December 2, 2025

DOI: 10.3892/mco.2026.2951

Abstract. Programmed cell death (PCD) and cellular immunity play pivotal roles in colorectal cancer (CRC) progression; understanding their crosstalk and identifying key genes could improve risk stratification and therapy. A univariate Cox analysis was performed to identify PCD-related genes (PRGs) and immune-related genes (IRGs) that are significantly associated with prognosis. Through principal component analysis (PCA), the immune and PCD levels were assessed in individual tumor tissues, subsequently categorizing patients into distinct molecular subtypes. Using the TCGA-COAD dataset as the training set and GSE17538 and GSE29621 as validation sets, machine learning model construction was performed. Leveraging the expression matrix of PRGs and IRGs, 101 machine learning models were constructed, with CoxBoost + Ridge emerging as the best-performing model. The model construction was based on previously reported methodology proposed, integrating 10 machine learning algorithms to form distinct models. The best model generated a risk score, referred to as the 'Score'. Additionally, the association between the 13 feature genes included in the Score and both prognosis and the tumor microenvironment (TME) were analyzed. Finally, experimental validation of the LTB4R gene was performed using western blotting and immunohistochemistry methods. In various datasets, PCA categorized patients into four molecular subtypes, with the immune potential index_low + PCD potential index_low group showing the highest survival rate. Among the 101 machine learning models developed, the CoxBoost + Ridge model demonstrated the best predictive performance. The Score generated by this model effectively stratified patients into high and low groups. Notably, significant differences were observed between the two groups in terms of TME, response to immunotherapy, and mutated genes. Additionally, a detailed analysis of the relationships between different feature genes, prognosis, and tumor immunity were conducted. In conclusion, the predictive model and risk score developed reflect the impact of the crosstalk between cellular immunity and PCD on the prognosis of CRC. Key genes in this crosstalk represent potential therapeutic targets, while our model provides a tool for TME evaluation and immunotherapy response prediction in CRC.

Correspondence to: Dr Qiumei Wu, Oncology Department 1, Central People's Hospital of Zhanjiang, 236, Yuan Zhu Road, Zhanjiang, Guangdong 524000, P.R. China
E-mail: 13763037770@163.com

Abbreviations: C-index, consistency index; CNV, copy number variation; CRC, colorectal cancer; DEGs, differentially expressed genes; Fges, functional gene expression signatures; GEO, Gene Expression Omnibus; HSPB1, heat shock protein β-1; ICI, immune checkpoint inhibitor; IPI, immune potential index; IRGs, immune-related genes; K-M, Kaplan-Meier; MDSC, myeloid-derived suppressor cells; MHC, major histocompatibility complex; MSI, microsatellite instability; OS, overall survival; PCA, principal component analysis; PCD, cellular programmed cell death; PPI, PCD potential index; PRGs, PCD-related genes; TCGA, The Cancer Genome Atlas; TIDE, tumor immune dysfunction and exclusion; TME, tumor microenvironment; TAM.M2, tumor-associated M2 macrophages

Key words: PCD, cellular immune, CRC, prognosis, TME, immunotherapy response

Introduction

Cancer is the second most lethal disease worldwide, with colorectal cancer (CRC) being the third most common and deadly cancer in western countries (1). Late-stage metastasis is the main cause of death among patients with CRC. CRC demonstrates significant heterogeneity both within and between tumors. Despite the numerous types and subtypes of colon cancer, once distant metastasis occurs, the long-term survival prospects for patients are very limited. Effective treatment options for late-stage colon cancer remain scarce. While immune checkpoint inhibitor (ICI) can induce remission in CRC with high microsatellite instability (MSI) (2), there are certain limitations, including individual variations in treatment sensitivity and the potential for post-treatment drug resistance. Therefore, accurately predicting the prognosis of patients with CRC is essential for effective treatment and clinical management of this disease.

Programmed cell death (PCD) is an evolutionarily conserved process of cellular suicide that is controlled by the interplay of multiple genes and signaling pathways. PCD

encompasses numerous biological processes of cell death, including apoptosis, pyroptosis, ferroptosis, autophagy, necroptosis, cuproptosis, parthanatos, entotic cell death, netotic cell death, lysosome-dependent cell death, alkaliptosis, and oxeiptosis. A recent study has demonstrated that several types of atypical PCD, including ferroptosis, pyroptosis, necroptosis, parthanatos and oxeiptosis, are closely associated with the occurrence and development of cancers such as colon cancer (3). PCD can have a dual role in tumor development, either promoting or inhibiting tumor growth depending on the cellular contents released during the process. Additionally, PCD is intricately linked to the immune system, as it can regulate the effect or enrichment of immune cells, thereby participating in the fine-tuning of anti-tumor immunity within the tumor microenvironment (TME). Liu *et al* (4) reported that apoptosis, necroptosis, pyroptosis, ferroptosis, and autophagy play crucial roles in regulating the immunosuppressive TME and influencing clinical outcomes of cancer treatments. Wu *et al* (5) elucidated the impact of cytokines produced by inflammasomes and pyroptosis on the breast cancer TME, and improved immunotherapy efficiency for breast cancer based on insights from pyroptosis. Some researchers have constructed risk models using gene combinations associated with PCD to predict the efficacy of immunotherapy for lung squamous cell carcinoma (6). These findings highlight the significant interaction between tumor immunity and PCD.

In the present study, the crosstalk between cellular immunity and PCD was explored. The objective was to develop a risk prediction model for CRC based on the effects of both cellular immunity and PCD. This model aimed to assess patient prognosis, enhance risk stratification, and improve clinical management of patients with CRC. The critical relationship between cellular immunity and PCD was uncovered, identifying key genes that influence patient prognosis, and providing novel therapeutic targets for patients with CRC.

Materials and methods

Data acquisition. The gene expression data and related clinical information for The Cancer Genome Atlas (TCGA)-colon adenocarcinoma (COAD) were sourced from TCGA database (https://portal.gdc.cancer.gov/). Immune-related genes (IRGs) were downloaded from the IMMPORT (https://www.immport.org/home) database, while PCD-related genes (PRGs) were referenced from the recent study by Zou *et al* (7). Genetic mutation data were obtained from the Genomic Data Commons (GDC; https://portal.gdc.cancer.gov/) database and analyzed using the 'maftools' package. Transcriptome datasets GSE17538, GSE29621, GSE39582, GSE44076 and GSE74602 were retrieved from the Gene Expression Omnibus (GEO) database. Additionally, GSE161277 was downloaded for single-cell RNA sequencing (scRNA-seq) data. Due to the small sample sizes of GSE39582, GSE44076 and GSE74602, they were merged and normalized into the GEO-Meta dataset for model validation.

Computational model for evaluating the levels of PCD and immunity in CRC. Zhou *et al* (8) developed the apoptosis index and epithelial-mesenchymal transition (EMT) index to assess the prognosis of COAD. Based on their study, the Immune Potential Index (IPI) and PCD potential index (PPI) were introduced in the present study. Using the TCGA-COAD dataset, immune and PCD genes were utilized as independent variables, with overall survival (OS) as the target variable, to identify significant genes associated with prognosis through univariate Cox regression analysis. In the TCGA-COAD dataset, differentially expressed genes (DEGs) between tumors and normal tissues were first identified. These DEGs were then combined with significant genes from the univariate Cox regression analysis to pinpoint IRGs and PRGs. At the same time, these genes were intersected with those from the GSE17538, GSE29621, GSE39582, GSE44076 and GSE74602 datasets to identify IRGs and PRGs that present across all datasets.

Principal component analysis (PCA) was employed to quantify the levels of immunity and PCD in each tumor tissue, with main components 1 and 2 serving as the primary dimensions. Referring to previous research (9), the IPI and PPI were defined respectively, where the formula for calculating IPI or PPI is $\sum$ (|PC1i| + |PC2i|), with i representing the gene expression matrix of IRGs or PRGs. Patients in the TCGA-COAD and GSE17538 datasets were divided into two molecular subtypes based on the median values of IPI: IPI_high and IPI_low, while they are also divided into another two molecular subtypes based on the median values of PPI: PPI_high and PPI_low. Combing IPI and PPI, patients were divided into four molecular subtypes: IPI_high + PPI_high, IPI_high + PPI_low, IPI_low + PPI_high, and IPI_low + PPI_low. Kaplan-Meier (K-M) curve analysis was used to compare OS differences among these four molecular subtypes.

Crosstalk of IRG and PRG and development of risk scoring model. Based on the merged expression matrix of IRGs and PRGs, clustering analysis on the GSE17538 and TCGA-COAD datasets was conducted using the R package 'ConsensusClusterPlus'. The association between the identified clustering categories and OS was then investigated.

To develop a high-precision and stable risk assessment model, the study of Liu *et al* (10) was referenced, and a combination of 101 algorithms was constructed by integrating 10 machine learning algorithms. The machine learning algorithms include random survival forest, elastic network, least absolute shrinkage and selection operator, Ridge, stepwise Cox, CoxBoost, partial least squares regression for Cox, supervised principal components, generalized boosted regression modeling and survival support vector machine. Details of the hyperparameters used in the machine learning models are provided in Table SI. A leave-one-out cross-validation framework was employed to fit these 101 prediction models, using a merged gene set of IRGs and PRGs as independent variables, with the TCGA-COAD dataset serving as the training set. At the same time, the consistency index (C-index) for each model was calculated across all validation datasets (GSE17538 and GSE29621). The model with the highest weighted average C-index in the validation set was selected as the best model. The code for model training and validation has been uploaded to https://github.com/wuqiumei/101-ML.git.

Using this optimal model, a risk score was calculated for each sample, referred to as 'Score'. Samples from different datasets were divided into high and low groups based on the

median value of Score. The value of Score was validated in the GSE17538, GSE29621 and TCGA-COAD datasets. Based on the TCGA-COAD dataset, a nomogram integrating the Score with other clinical factors was constructed to evaluate its predictive ability for 1-year, 3-year and 5-year survival rates. Additionally, the Score was explored in relation to various aspects such as TME, immune markers and genetic mutations based on the TCGA dataset.

Tumor immune-related analysis. The 'estimate' R package is used to calculate the Immune Score and Stromal Score of patients. The 'xCell' R package is used to assess the infiltration of various immune cell types in both groups with high and low scores. Additionally, Bagaev *et al* (11) proposed 29 functional gene expression signatures (Fges) to represent the cellular and functional attributes of the TME.

Investigation of immunotherapy response. Based on the TCGA-COAD dataset, the Tumor Immune Dysfunction and Exclusion (TIDE) tool (http://tide.dfci.harvard.edu/login/) was employed to assess the potential individual response to ICI treatment (12). Individual scores such as Exclusion score, myeloid-derived suppressor cells' (MDSCs) score, tumor-associated M2 macrophages' (TAM) score and cancer-associated fibroblasts' (CAFs) score were also obtained.

Investigation of genes included in the model. Based on the TCGA dataset, the differential expression of genes included in the model between tumors and normal tissues was investigated. Underlying reasons for these differential expression levels from the perspectives of genetic mutations, copy number variations (CNV) and methylation were explored. Additionally, the expression association of the included genes with tumor immune genes was explored from multiple aspects such as chemokines, immune inhibitors, Major Histocompatibility Complex (MHC), immune stimulants and receptor-related genes.

Single-cell analysis. The single-cell sequencing dataset GSE161277 was retrieved from the GEO database. Low-quality cells were excluded based on the criteria of nFeature_RNA >500, nFeature_RNA <10,000, and percent.mt <25. The 'harmony' package was used to preprocess and integrate four single-cell samples. The CellCycleScoring function was used to calculate the cell cycle scores, and the influence of the cell cycle on clustering was subsequently removed. The FindVariableFeatures function in the 'Seurat' R package was used to identify 2,000 highly variable genes for subsequent dimension reduction based on PCA. According to principal components 1 to 20, the t-distributed stochastic neighbor embedding method was employed to visualize visualizing single-cell clustering. Subsequently, the 'singleR' R package was used to annotate cells based on different markers on the cell surface.

Specimen collection and LTB4R expression detection. Patients who received treatment for CRC in the Department of Gastrointestinal Surgery at Zhanjiang Central People's Hospital from November 2021 to November 2022 were selected as research subjects. The patients ranged in age from 34 to 78 years, with male and female patient percentages of 72.5 and 27.5%, respectively. Inclusion criteria were as follows: i) Age ≥18 years; ii) Confirmed diagnosis of CRC through pathological examination, without other tissue-originated malignant tumors; iii) no peripheral organ metastasis before surgery and underwent radical tumor surgery with 1-year follow-up. Patients with clear peripheral organ metastasis or recurrence within 1 year of follow-up, as evidenced by imaging or pathology, were classified into the transfer group. Otherwise, they were classified into the non-transfer group. From the transfer group, 10 patients were randomly selected and matched with 10 patients from the non-metastasis group based on propensity scores considering factors such as sex, age, body mass index and tumor staging. The operation process of propensity score matching was completed using SPSS 21.0 software (IBM Corp.). CRC specimens from these two groups were obtained retrospectively from the specimen library for immunohistochemistry (IHC) and western blotting to assess LTB4R expression. The present study adhered to the Helsinki Declaration and was approved by the Institutional Review Committee of Zhanjiang Central People's Hospital (approval no. 2023-002-013; Zhanjiang, China). Written informed consent was provided by all participants.

IHC. CRC tissue samples were collected, including 10 cases from the transfer group and 10 matched cases from the non-transfer group. The tissue was typically embedded in paraffin and sectioned (4-μm thick). Deparaffinization was performed using xylene, followed by rehydration with a gradient of alcohols. The sections were then placed in TRIS-EDTA antigen retrieval solution, covered, and microwaved for 10 min on high power and 5 min on medium power. After stopping the heating, the sections were cooled to room temperature and washed several times with distilled water. Endogenous peroxidase activity was blocked using 3% H_2O_2 at room temperature for 10 min. The sections were incubated overnight at 4˚C with a primary antibody against LTB4R (1:25; cat. no. R30118; Zen-Bio, Inc.). The next day, the sections were rewarmed at room temperature for 45 min, washed three times with PBS, and incubated with a biotinylated secondary antibody. The staining was visualized using DAB, followed by counterstaining with hematoxylin and differentiation with hydrochloric acid alcohol. Finally, the sections were dehydrated in a gradient of ethanol, cleared in xylene, and mounted for microscopic examination.

Western blot analysis. Total protein was extracted from CRC tissue. Protein concentration was determined using the BCA method, and the samples were stored at -80˚C. A total of, 20 μg proteins were separated by 10% SDS-PAGE gel electrophoresis and transferred onto a PVDF membrane using a constant current of 300 mA. The membrane was blocked with a blocking solution at room temperature for 1 h. The blocking solution was prepared by dissolving non-fat milk in TBST (containing 0.05% Tween-20) to a final concentration of 5%. The membrane was then incubated overnight at 4˚C with diluted primary antibodies: LTB4R (1:1,000) and GAPDH (1:50,000; cat. no. 60004-1-Ig; Proteintech Group, Inc.). After

washing with TBST, the membrane was incubated with an HRP-conjugated secondary antibody (1:50,000; cat. no. BL003A; Biosharp Life Sciences) at room temperature for 1-2 h. Following additional washes, chemiluminescent detection was performed using a chemiluminescence substrate (cat. no. BL520A; Biosharp Life Sciences). Protein band intensities were analyzed using ImageJ software (version: 1.8.0; National institutes of Health), with GAPDH as the internal reference for comparing protein expression differences between different groups.

Statistical analysis. The Wilcoxon test was used to compare differences between continuous variables. while the chi-square test was employed for inter-group comparisons of categorical variables. The log rank test was utilized to analyze inter-group differences in survival rates. Depending on the data characteristics, Pearson correlation coefficient or Spearman correlation coefficient was used for correlation analysis. $P<0.05$ was considered to indicate a statistically significant difference ($^{*}P<0.05$; $^{**}P<0.01$; $^{***}P<0.001$; $^{****}P<0.0001$).

Results

Identifying the differentially expressed IRGs and PRGs associated with OS. A total of 2,483 IRGs were downloaded from the IMMPORT database (Table SII), and referred to the research by Zou *et al* (7) to obtain 1277 genes related to 12 types of PCD (Table SIII). Using the TCGA-COAD dataset, univariate Cox analysis was performed with OS time as the target variable and 135 immune genes (Table SIV) and 102 PCD genes (Table SV) that are related to prognosis were identified. The final IRGs and PRGs were obtained by selecting genes that exist in all datasets including GSE17538, GSE29621, GSE39582, GSE44076 and GSE74602.

Based on the TCGA-COAD dataset, the heatmaps of DEGs were generated for IRGs and PRGs between tumor tissues and adjacent normal tissues (Fig. 1A and B). Similarly, heatmaps of DEGs between tumors and adjacent tissues were obtained from the GEO-Meta dataset (Fig. 1C and D). After combining the gene expression matrix for IRGs and PRGs, consensus clustering analysis on the GSE17538 dataset was performed (Fig. 1G). The results revealed significant differences in OS rates among different clusters (Fig. 1H). The same analysis conducted on the TCGA-COAD dataset (Fig. 1E and F) also demonstrated significant differences in OS among different clusters ($P<0.05$). These findings suggested that the gene set comprising IRGs and PRGs can effectively distinguish the overall prognosis of colon cancer to a certain extent.

Construction of IPI and PPI. To further investigate the crosstalk between IRGs and PRGs, PCA was performed to quantify the immune level and PCD level in each tumor tissue, which are defined as IPI and PPI, respectively. The distributions of IPI and PPI are shown in Fig. 2A and B; the correlation analysis between IPI and PPI is presented in Fig. 2C. Survival analysis of the TCGA-COAD dataset revealed that the IPI_high group had a significantly lower survival rate compared with the IPI_low group ($P<0.01$; Fig. 2D). Similarly, the PPI_high group had a significantly reduced survival rate compared with the PPI_low group ($P<0.01$; Fig. 2E), indicating that both high PPI and high IPI are associated with poorer survival outcomes.

Based on IPI and PPI, patients in the TCGA-COAD dataset were categorized into four molecular subtypes: IPI_high + PPI_high, IPI_high + PPI_low, IPI_low + PPI_high, and IPI_low + PPI_low. K-M analysis demonstrated that the survival rates of the IPI_high + PPI_high, IPI_high + PPI_low, and IPI_low + PPI_high subtypes were significantly lower than those of the IPI_low + PPI_low subtype ($P<0.001$; Fig. 2F). After merging the first three subtypes into a single category called the 'Others group', a comparison with the IPI_low + PPI_low subtype revealed consistent results (Fig. 2G). The results of the multivariate Cox regression analysis (Fig. S1) based on TCGA-COAD data indicated that this molecular classification is an independent prognostic factor, unaffected by variables such as age, tumor stage, and microsatellite status. Survival analysis results for IPI and PPI based on the GSE17538 dataset are depicted in Fig. 2H and I, respectively. As shown in Fig. 2J, the IPI_low + PPI_low group has a higher survival rate. However, due to limitations in the dataset samples, this difference has not yet reached statistical significance. The analysis across various datasets indicates a crosstalk between immune and PCD. The combination of IPI and PPI effectively distinguishes OS rates and other prognostic factors in patients with CRC.

Development of machine learning models. After merging IRGs and PRGs, an expression matrix containing 104 genes was constructed. Using this combined gene set as the independent variable and the TCGA-COAD dataset as the training set, 101 prediction models were fitted, and the C-index was calculated for each model in the validation datasets (GSE17538 and GSE29621). The performance of these prediction models is presented in Fig. 3A, which reveals that the CoxBoost + Ridge model achieved the highest weighted average C-index in the validation set. This model includes 13 gene features: VEGFA, CCRL2, LTB4R, RORC, INHBB, FABP4, NOS2, C8G, CD24, HSPB1, SFRP2, STK25 and NOL3. The risk score for each sample was calculated. Using the median value of Score, samples from different datasets were classified into high and low groups. The K-M analysis results for the TCGA-COAD, GSE17538 and GSE29621 datasets are depicted in Fig. 3B-D respectively, demonstrating that the prognosis of the high group was significantly worse. To explore the performance of Score in predicting OS in the GSE17538 dataset, it was found that AUC for 1-year, 3-year and 5-year OS was 0.792, 0.716 and 0.758, respectively (Fig. 3F). In the GSE29621 dataset, the AUCs for 1-year, 3-year and 5-year survival rates were 0.645, 0.604 and 0.623, respectively (Fig. 3E). Simultaneously, a multivariate Cox regression analysis based on the TCGA-COAD dataset revealed that the Score is a significant prognostic factor, independent of tumor grading, age and MSI (Fig. 3G). A nomogram incorporating the Score and other clinical factors was also constructed (Fig. 3H). The receiver operating characteristic curve areas for predicting 1-year, 3-year, and 5-year OS were 0.759, 0.797 and 0.791, respectively (Fig. 3I), indicating strong predictive performance.

TME of high and low score groups. TME is a complex environment comprising tumor cells, immune cells and stromal cells, all of which significantly affect tumor cell invasion and metabolism (13). Analysis of the TCGA-COAD dataset using the ESTIMATE algorithm revealed the Immune Score

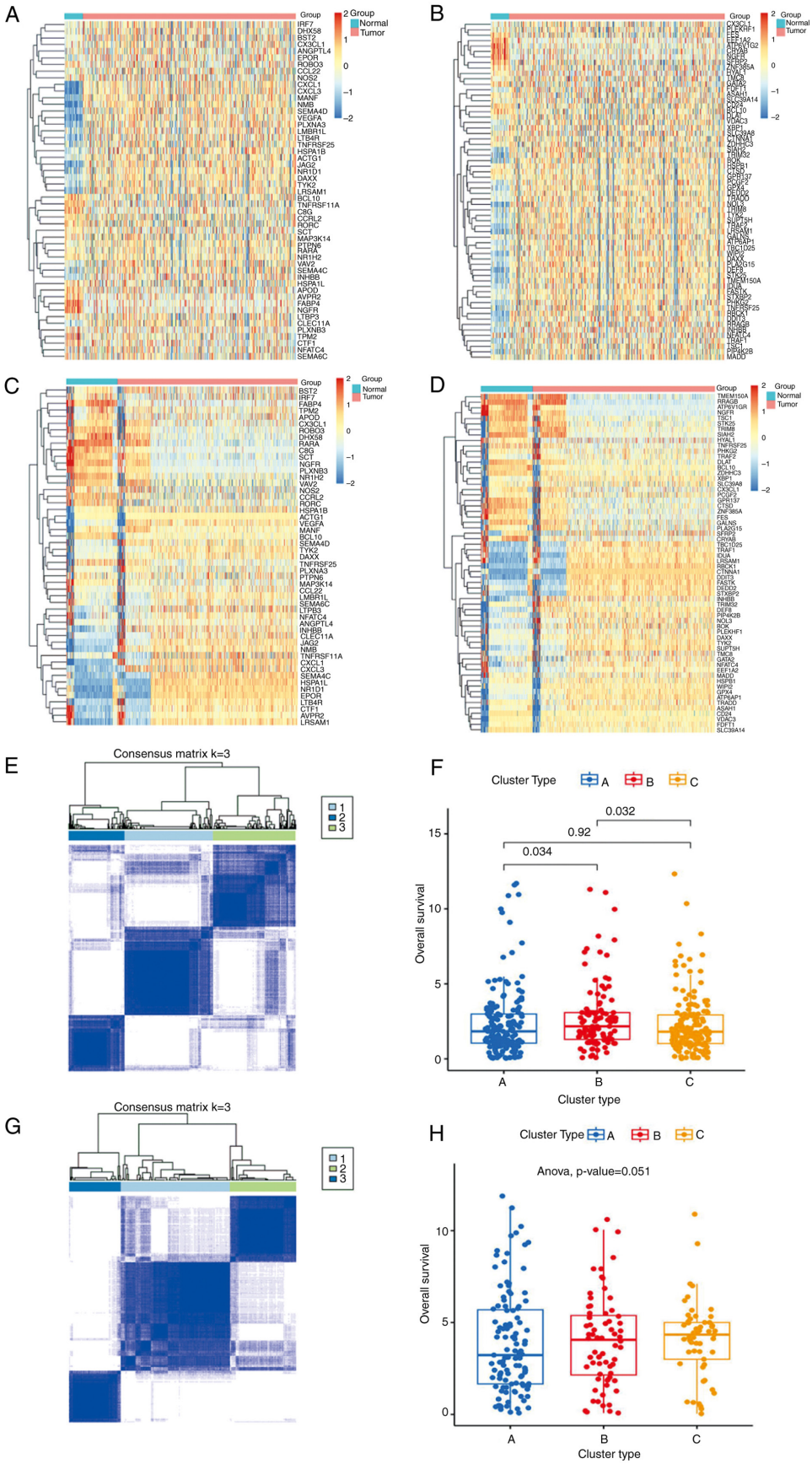

Figure 1. IRGs and PRGs associated with OS. (A) Heatmap of IRGs in tumor and normal tissues from the TCGA-COAD dataset. (B) Heatmap of PRGs in tumor and normal tissues from the TCGA-COAD dataset. (C) Heatmap of IRGs in tumor and normal tissues from the GEO-Meta dataset. (D) Heatmap of PRGs in tumor and normal tissues from the GEO-Meta dataset. (E) Consensus clustering of the TCGA-COAD dataset based on the merged expression matrix of IRGs and PRGs. (F) Box plots comparing OS time across different clusters in the TCGA-COAD dataset. (G) Consensus clustering of the GSE17538 dataset based on the merged expression matrix of IRGs and PRGs. (H) Box plots comparing OS time across different clusters in the GSE17538 dataset. IRGs, immune-related genes; PRGs, PCD-related genes; TCGA, The Cancer Genome Atlas; COAD, colon adenocarcinoma; GEO, Gene Expression Omnibus; OS, overall survival.

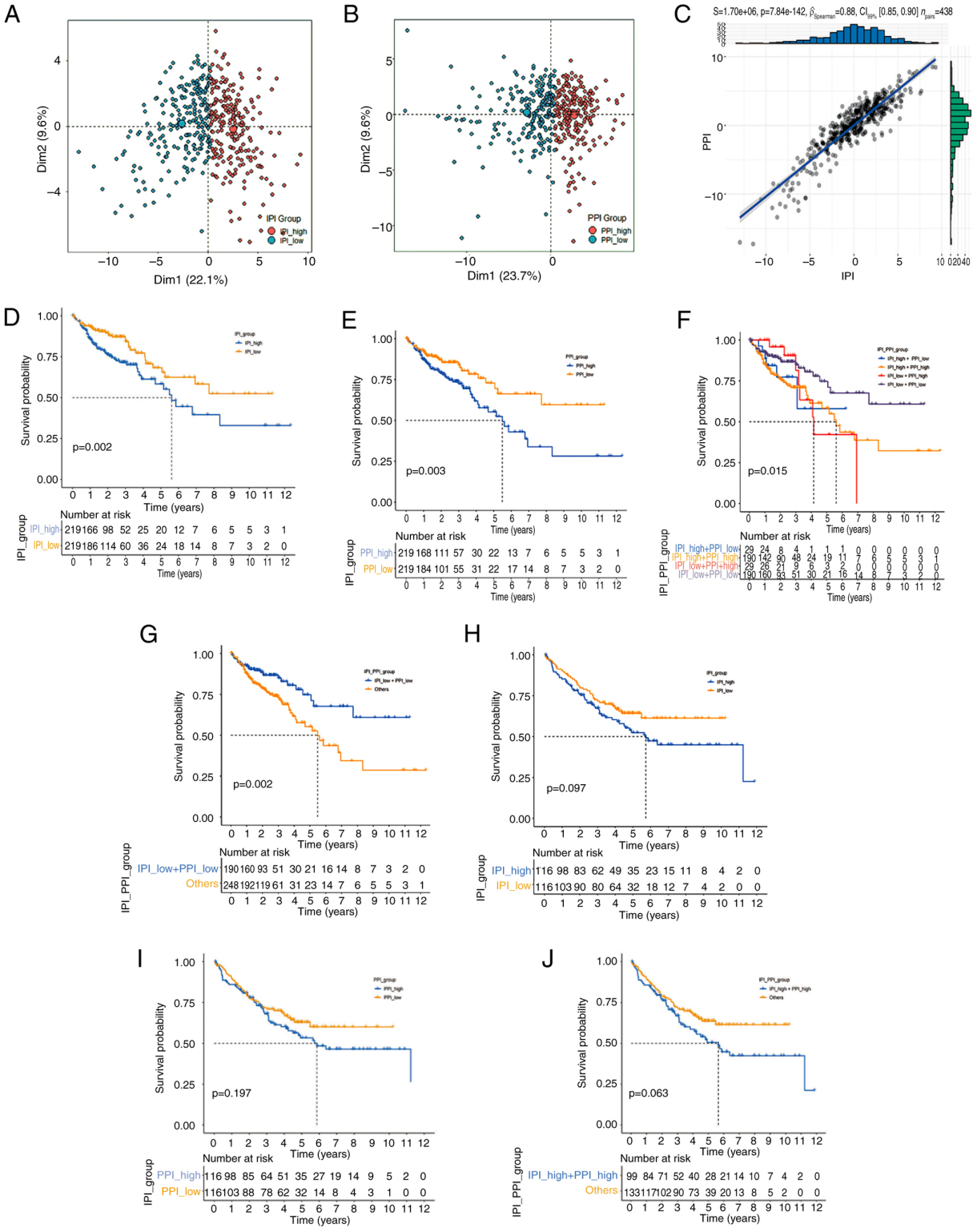

Figure 2. IPI and PPI. (A) PCA distribution plot of IPI in the TCGA-COAD dataset. (B) PCA distribution plot of PPI in the TCGA-COAD dataset. (C) Scatter plot showing the correlation between IPI and PPI in the TCGA-COAD dataset. (D) K-M analysis results for high and low IPI subgroups in the TCGA-COAD dataset. (E) K-M analysis results for high and low PPI subgroups in the TCGA-COAD dataset. (F) K-M analysis results for four subgroups in the TCGA-COAD dataset. (G) K-M analysis results comparing the IPI_low + PPI_low subgroup with other subgroups in the TCGA-COAD dataset. (H) K-M analysis results for IPI high and low subgroups in the GSE17538 dataset. (I) K-M analysis results for PPI high and low subgroups in the GSE17538 dataset. (J) K-M analysis results comparing the IPI_low and PPI_low subgroups with other subgroups in the GSE17538 dataset. PCA, principal component analysis; IPI, immune potential index; TCGA, The Cancer Genome Atlas; COAD, colon adenocarcinoma; PPI, PCD potential index; K-M, Kaplan-Meier.

of the low Score group was significantly higher than that of the high Score group (P<0.05, Fig. 4A), suggesting greater immune cell infiltration in the low Score group. As shown in Fig. 4B, the Stromal Score of the low Score group was significantly lower than the high group (P<0.01). Using the XCELL algorithm to assess and compare immune cell

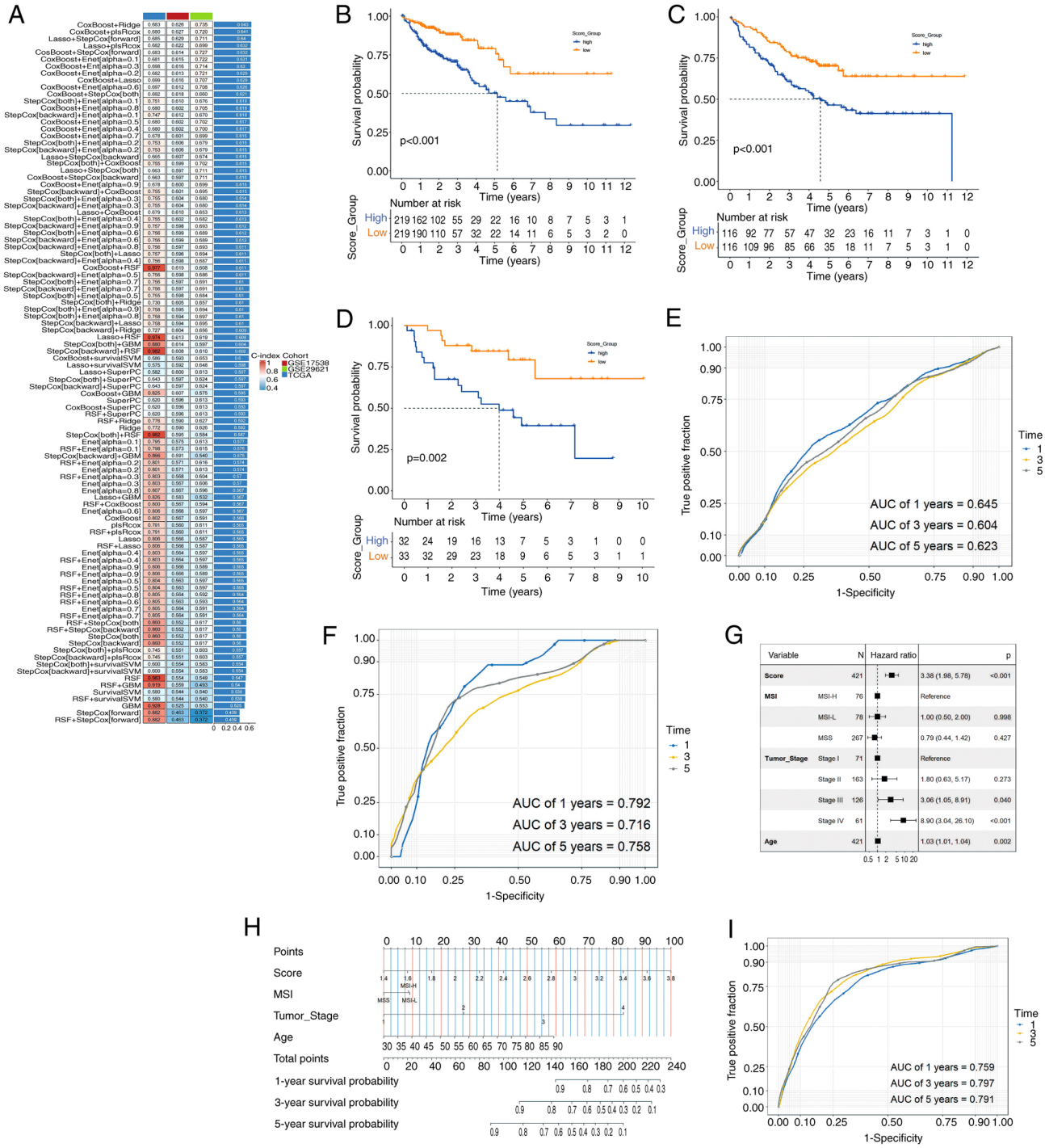

Figure 3. Performance of machine learning models and Score in prognostic prediction. (A) Consistency index comparison across different machine learning models in three datasets. (B) K-M analysis results for high and low Score subgroups in the TCGA-COAD dataset. (C) K-M analysis results for high and low Score subgroups in the GSE17538 dataset. (D) K-M analysis results for high and low Score subgroups in the GSE29621 dataset. (E) ROC curves of Score for predicting 1-year, 3-year, and 5-year OS rates in the GSE17538 dataset. (F) ROC curves of Score for predicting 1-year, 3-year, and 5-year survival rates in the GSE29621 dataset. (G) Forest plot showing multivariate Cox regression results of Score and other clinical variables in the TCGA-COAD dataset, with time OS as the target variable. (H) Nomogram constructed using Score and other clinical variables. (I) ROC curves of nomogram for predicting 1-year, 3-year and 5-year survival in the TCGA-COAD dataset. KM, Kaplan-Meier; TCGA, The Cancer Genome Atlas; COAD, colon adenocarcinoma; ROC, Receiver Operating Characteristic; OS, overall survival; AUC, area under the curve.

infiltration between the two groups, it was observed that the low Score group had higher abundances of activated dendritic cells, B cells, CD4$^+$ memory T cells, CD8$^+$ naive T cells, CD8$^+$ T cells, CD8$^+$ Tcm cells, CD4$^+$ T cells, CD4$^+$ Tem cells, CD8$^+$ memory T cells, natural killer (NK) cells, and others (Fig. 4C). Further correlation analysis indicated that the Score was negatively associated with the infiltration of 12 types of immune cells, including macrophages, activated dendritic cells, memory B cells, T cells, Th2 cells, CD8$^+$ Tcm cells and NK cells (Fig. 4D). This analysis supports the conclusion that a higher Score is linked to reduced immune cell infiltration.

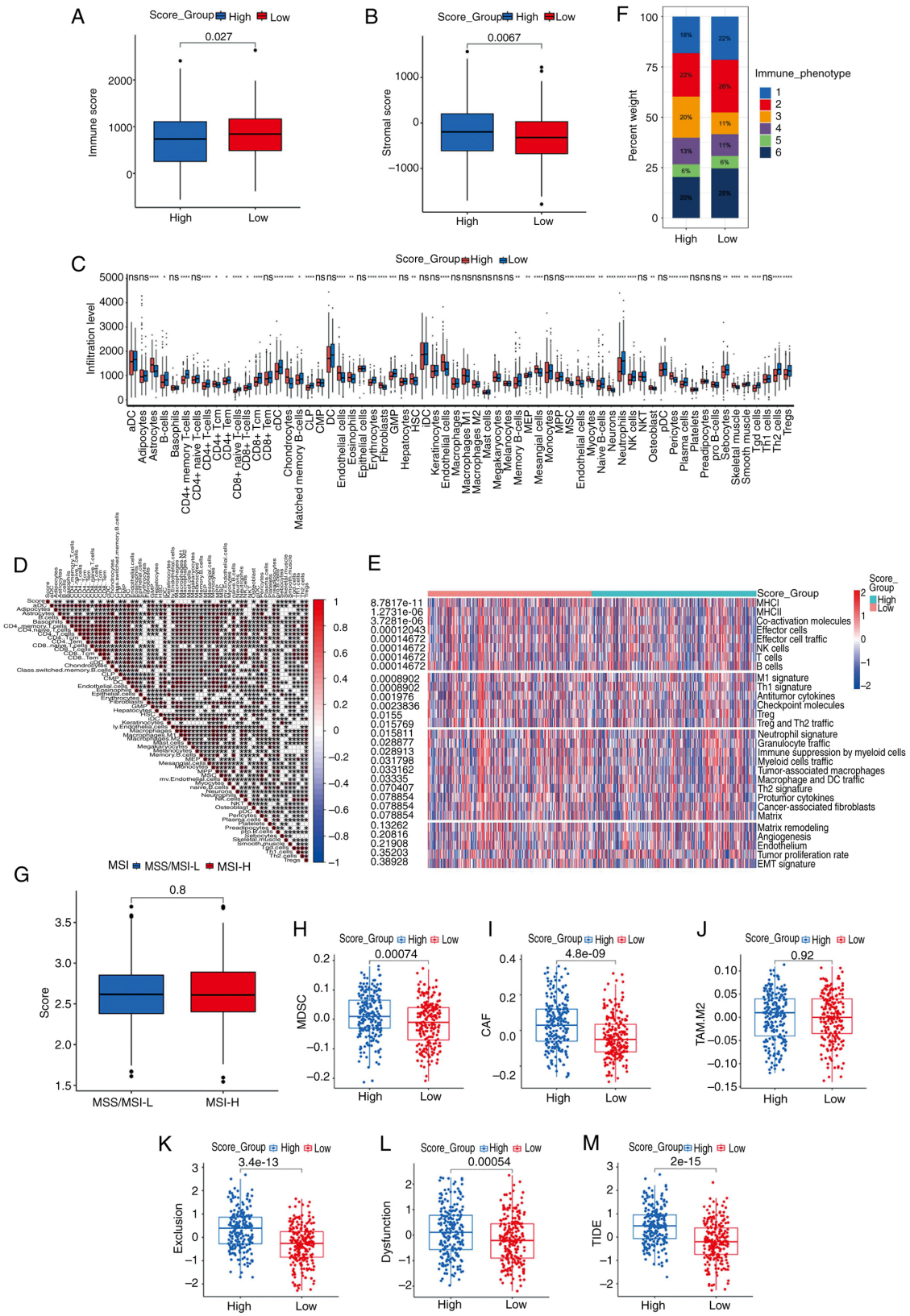

Figure 4. Comparison of the tumor microenvironment between high and low Score groups. (A) Box plots comparing Immune Score between high and low Score groups in the TCGA-COAD dataset (using ESTIMATE algorithm). (B) Box plots comparing Stromal Score between two groups in the TCGA-COAD dataset (using ESTIMATE algorithm). (C) Box plots showing immune cell infiltration in high and low Score groups in the TCGA-COAD dataset (using XCELL algorithm). (D) Correlation graph between Score and various immune cells in the TCGA-COAD dataset. (E) Heatmap comparing 29 functional gene expression signatures between high and low Score groups in the TCGA-COAD dataset. (F) Comparative analysis of different immune subtypes between two groups in the TCGA-COAD dataset. (G) Comparison of Score across different MSI subtypes in the TCGA-COAD dataset. (H) Comparison of MDSCs between high and low Score groups. (I) Comparison of CAFs between the two groups. (J) Comparison of TAM.M2 between the two groups. (K) Comparison of Exclusion Score between the two groups. (L) Comparison of Dysfunction Score between the two groups. (M) Comparison of TIDE scores between the two groups. TCGA, The Cancer Genome Atlas; COAD, colon adenocarcinoma; MSI, microsatellite instability; MDSCs, myeloid-derived suppressor cells; CAFs, cancer-associated fibroblasts; TAM.M2, tumor-associated M2 macrophages; TIDE, tumor immune dysfunction and exclusion; MSS, microsatellite stable. *P<0.05; **P<0.01; ***P<0.001; ****P<0.0001.

The scores of 29 Fges were compared between the two groups, and it was found that the low Score group exhibited significantly higher scores in antitumor immune-related Fges, including M1 signature, myeloid immune suppression, checkpoint molecules, Th2 signature, neutrophil signature, antitumor cytokines, NK cells, Th1 signature and T cells (Fig. 4E). The TCGA-COAD dataset defines three immune phenotypes: Desert phenotype (phenotype 1 and 2), excluded phenotype (phenotype 3 and 4) and inflamed phenotype (phenotype 5 and 6). As depicted in Fig. 4F, the proportions of desert phenotype (40%) and excluded phenotype (33%) in the high Score group were higher than those in the low Score group (48 and 22%, respectively), while the proportion of inflamed phenotype (31%) was lower compared with the low Score group (26%). A chi-square test performed on the two groups of immune phenotypes yielded a P-value of 0.036, indicating a significant difference in the proportion of immune phenotypes between the two groups (P<0.05).

The present study further investigated the association between Score and immunotherapy response. Given the correlation between immunotherapy response and MSI, the association between Score and MSI was explored. As demonstrated in Fig. 4G, there was no significant difference in Score between the microsatellite stable (MSS)/MSI low subtype and the MSI high (MSI-H) subtype in the TCGA-COAD dataset. The high Score group exhibited significantly higher scores for MDSC, CAF, TAM.M2, Exclusion and Dysfunction compared with the low Score group (P<0.05; Fig. 4H-L). This indicates that the high Score group is more prone to tumor immune evasion. Furthermore, the TIDE score of the high Score group was significantly higher than that of the low Score group (P<0.001; Fig. 4M), suggesting a lower response to ICI treatment in the high Score group.

Genetic alterations. Somatic mutations in the high and low Score groups in the TCGA-COAD dataset were further investigated. The waterfall plots for the two groups of mutated genes are shown in Fig. 5A and B, respectively. The results revealed that somatic mutations were present in 93.97% of samples in the low Score group and 98.02% of samples in the high Score group. The top 8 genes with the highest mutation frequencies were identical in both groups, including APC, TP53, PIK3CA, TTN, CRAS, MUC16, SYNE1 and FAT4. As depicted in Fig. 5C, there were notable differences in somatic gene mutations between the two groups. In the high Score group, mutations in TP53 (P<0.001), SNX1 (P<0.01), ZNF214 (P<0.01), ELAPOR1 (P<0.01), AP2M1 (P<0.01), LMX1A (P<0.01) and NACC2 (P<0.01) were notably higher compared with the low Score group. On the other hand, mutations in PCDH10 (P<0.001), WDR19 (P<0.001), SCN5A (P<0.01), ATP2 (P<0.01) and EFCAB13 (P<0.01) were greatly increased in the low Score group. The tumor-related signaling pathways were enriched by the mutated genes in the high and low Score groups, respectively 9 Fig. 5D and E). Both groups exhibited enrichment in largely the same signaling pathways, including RTK-RAS, NOTCH, WNT, Hippo, PI3K, Cell Cycle, MYC, TGF-β, TP53 and NRF2. Regarding tumor mutation burden, although the high Score group had a higher burden than the low Score group, this difference did not reach statistical significance (Fig. 5F).

Features genes included in the model. In total, 13 feature genes included in the model were analyzed. Using the expression matrix of these genes, the consensus clustering method was applied to the TCGA-COAD dataset. The optimal number of clusters k was determined to be 2, resulting in the division of the dataset samples into 2 clusters (Fig. 6A). The comparison of the OS time between different clusters is presented in Fig. 6B. Similarly, the GSE17538 dataset was clustered using the same method, and the optimal number of clusters k was also found to be 2 (Fig. 6C). Although differences in OS time between the clusters were observed, they did not reach statistical significance (Fig. 6D). In the TCGA-COAD dataset, K-M analysis of the 13 feature genes indicated that all were related to patient survival rate (Fig. 6E). Univariate Cox analysis revealed that VEGFA, LTB4R, INHBB, FABP4, C8G, HSPB1, STK25, and NOL3 were significant risk factors, whereas the remaining 5 feature genes were identified as significant protective factors (Fig. 6F). In the GSE17538 dataset, univariate Cox analysis showed that VEGFA, FABP4, HSPB1 and SFRP2 were significant risk factors, while RORC and NOS2 were significant protective factors (Fig. 6G). The differential expression of feature genes between tumor tissues and normal tissues in the TCGA-COAD dataset were further investigated. In cancer tissues, genes such as VEGFA, LTB4R, INHBB, STK25 and NOL3 were significantly upregulated, while protective factors including CCRL2, RORC, CD24 and SFRP2 were significantly downregulated (Fig. 6H). In the GSE17538 dataset, risk factors VEGFA and HSPB1 were significantly upregulated in cancer tissues, while protective factors CCRL2, RORC, NOS2, C8G, CD24 and STK25 were significantly downregulated (Fig. 6I). To explore the driving factors of abnormal expression of these feature genes in CRC tissues, the correlation was analyzed between gene expressions and mutations, methylation, and CNVs using the cBioPortal database. The results of this correlation analysis are shown in Fig. S2A-C. Additionally, the correlation analysis of feature gene expression is presented in Fig. S2D. The results indicated a broad positive correlation among VEGFA, LTB4R, INHBB, STK25 and NOL3, while CCRL2, RORC and CD24 also showed a positive correlation.

Association of feature genes with immunity. In the present study, the correlation between the expression of the 13 selected feature genes and various immune-related gene categories was analyzed, including chemokines, immune inhibitors, MHC-related genes, immune stimulation-related genes and receptor-related genes. The correlation analysis results, depicted in Fig. 7A-E, reveal a significant association between the expression of these 13 feature genes and these five types of immune genes. Specifically, genes such as SFRP2, NSO2 and FABP4 exhibit a positive correlation with the expression of most chemokines, immune inhibitors, MHC-related genes, immune stimulation-related genes and receptor-related genes. Conversely, the expression of genes like LTB4R shows a negative correlation with the expression of the majority of these IRGs.

Single-cell analysis results. Preprocessing, integration, dimensionality reduction and clustering analysis was performed on GSE161277. Using the R package 'singleR', cells were annotated based on various cell surface markers, ultimately

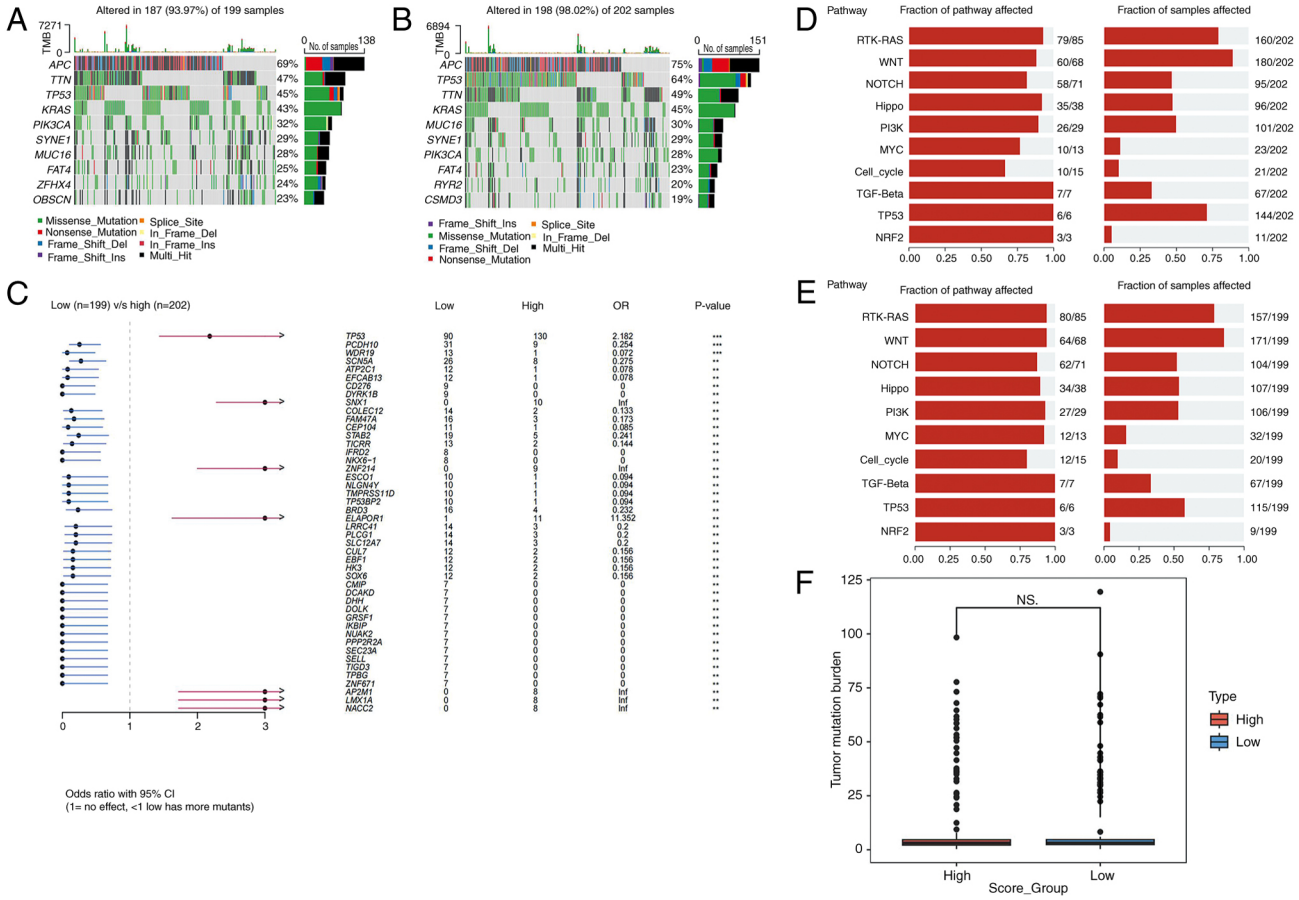

Figure 5. Comparison of the genetic mutation between high and low Score groups. (A) Waterfall plot of mutated genes in the low Score subgroup of the TCGA-COAD dataset. (B) Waterfall plot of mutated genes in the high Score subgroup. (C) Forest plot comparing mutated genes between the high and low Score subgroups in the TCGA-COAD dataset. (D) Significant enrichment pathways for mutated genes in the high Score subgroup. (E) Significant enrichment pathways for mutated genes in the low Score subgroup. (F) Box plot comparing tumor mutation burden between the high and low Score subgroups in the TCGA-COAD dataset. TCGA, The Cancer Genome Atlas; COAD, colon adenocarcinoma.

identifying 5 distinct cell types: epithelial cells, T cells, B cells, monocytes and endothelial cells (Fig. 8A). Comparison of the Score for each cell type (Fig. 8B) reveals obvious differences. Endothelial cells scored the highest, while B cells scored the lowest. This suggests that endothelial cells and B cells may play crucial roles in the crosstalk between cellular immunity and PCD. The expression levels of 13 feature genes in each cell subgroup are illustrated in Fig. 8C. Notably, VEGFA, STK25 and NOL3 are predominantly expressed in epithelial cells, while CD24 and other genes are mainly expressed in B cells and epithelial cells.

Analysis of LTB4R expression. IHC analysis revealed that the staining of LTB4R was markedly more intense in colon cancer tissues in the transfer group (Fig. 9A), while the staining was lighter in the non-transfer group (Fig. 9B). The results of the IHC analysis showed that the expression of LTB4R in the transfer group was significantly higher than that in the non-transfer group. Western blotting analysis showed that the LTB4R protein expression level was significantly higher in the transfer group compared with the non-transfer group (Fig. 9C and D), with a statistically significant difference ($P<0.01$) (Fig. 9E). These findings suggested that LTB4R expression levels may be useful in distinguishing between CRC recurrence and metastasis.

Discussion

PCD encompasses various processes, including apoptosis, pyroptosis, ferroptosis, autophagy, necroptosis, cuproptosis, parthanatos, entotic cell death, netotic cell death, lysosome-dependent cell death, alkaliptosis and oxeiptosis. The interplay among various PCD mechanisms is highly complex, characterized by numerous crosstalk interactions (14,15). Not only do they operate through distinct regulatory mechanisms individually, but they also mutually constrain and influence each other (15). These PCD pathways form a dynamic molecular interaction network, synergistically modulating cellular processes in cancer (16,17). Therefore, in the present study, various PCDs were investigated as a cohesive whole. Recent studies indicated that different forms of PCD, such as pyroptosis, necroptosis, parthanatos and oxeiptosis, play crucial roles in eliminating unnecessary cells and maintaining the health and stability of the body's microenvironment (4,18). However, the effects of PCD on tumor occurrence, invasion and immunity have not been thoroughly understood, and there remains considerable controversy in this area. On the one hand, PCD can promote the occurrence and progression of tumors under certain conditions. For example, ferroptosis-related genes can increase the survival rate of tumor cells by activating the TGFB pathway, and at the same

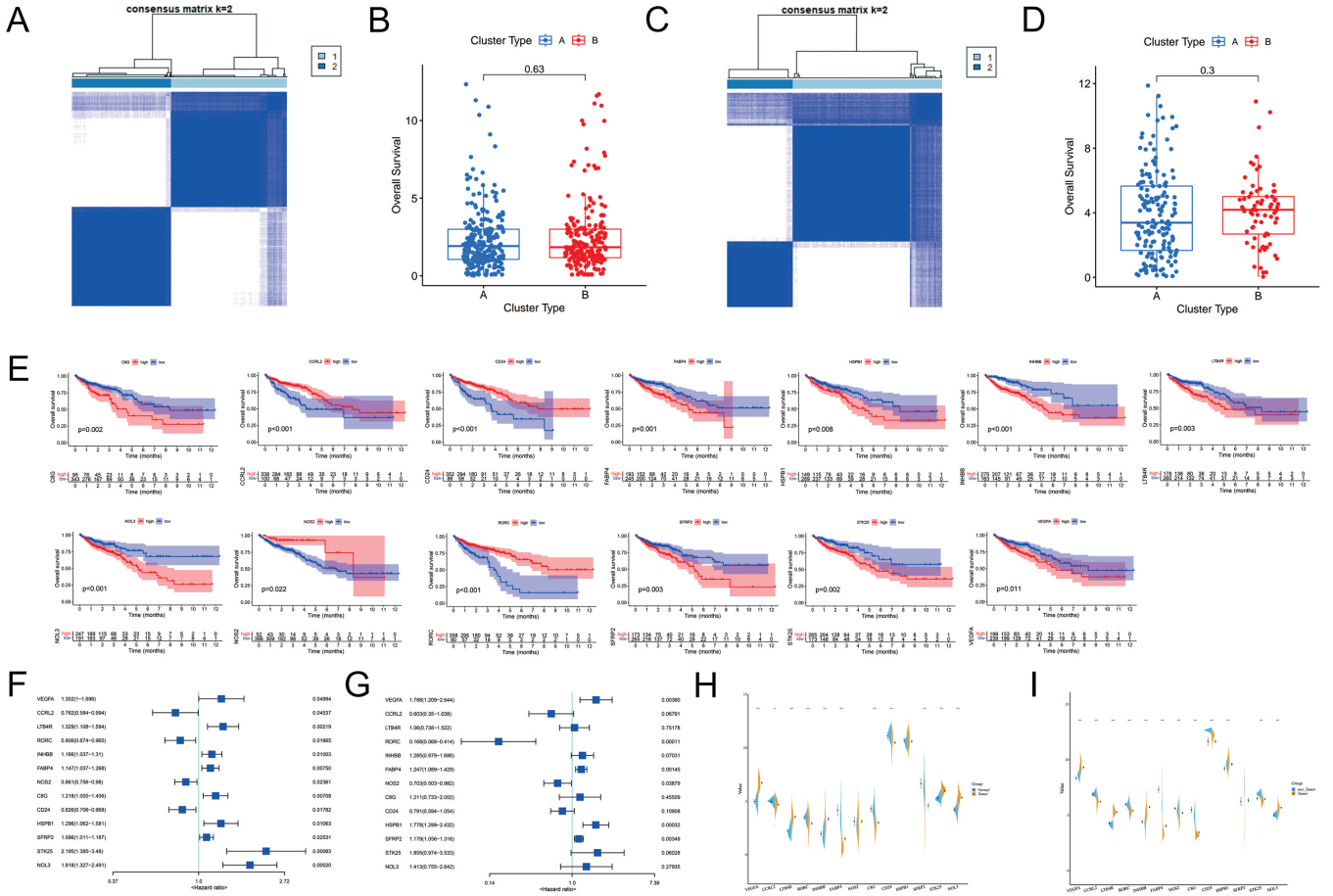

Figure 6. Analysis results of 13 feature genes. (A) Consensus clustering of the 13 feature genes in the TCGA-COAD dataset. (B) Box plot comparing OS time across different clusters in the TCGA-COAD dataset. (C) Consensus clustering of the 13 feature genes in the GSE17538 dataset. (D) Box plot comparing OS across different clusters in the GSE17538 dataset. (E) Kaplan-Meier analysis results for the 13 feature genes in the TCGA-COAD dataset. (F) Forest plot showing univariate Cox analysis results for the 13 feature genes in the TCGA-COAD dataset. (G) Forest plot showing univariate Cox analysis results for different feature genes in the GSE17538 dataset. (H) Violin plot comparing expression of feature genes between normal and tumor tissues in the TCGA-COAD dataset. (I) Violin plot showing expression comparison of feature genes between normal and tumor tissues in the GEO-Meta dataset. TCGA, The Cancer Genome Atlas; COAD, colon adenocarcinoma; OS, overall survival.

time accelerate the decomposition of the extracellular matrix, promoting tumor progression and invasion (18). On the other hand, PCD can regulate the enrichment of effector immune cells or regulatory immune cells, thereby playing a key role in regulating immunity, affecting TME, and influencing the clinical outcomes of cancer treatment (4). Currently, numerous studies have confirmed the close association among PCD, immunity and colon cancer prognosis (4,19). Exploring the crosstalk between PCD and cellular immunity in CRC can enhance the understanding of how these processes affect the prognostic mechanisms of CRC. The present study uncovered key genes that impact patient outcomes and identify potential therapeutic targets for CRC treatment.

In the present study, PCA algorithm was employed to reduce the dimensionality of expression matrix of IRGs and PRGs. IPI and PPI were then constructed to quantify immune levels and PCD levels in colon cancer tumor tissues. Based on IPI and PPI results, four molecular subtypes were classified and analyzed survival rate differences among these subtypes. It was found that the OS rate of the IPI_low + PPI_low group was significantly higher compared with the other groups. This analysis indicates a crosstalk between cellular immunity and PCD, and that combining IPI and PPI can effectively distinguish OS rates and other prognostic for patients with CRC. Based on the combined gene expression matrix of IRGs and PRGs, 101 machine learning models were constructed and a risk score named 'Score' was derived from the best-performing model. The Score demonstrated excellent prognostic performance in the TCGA-COAD, GSE17538 and GSE29621 datasets, indicating its effectiveness in reflecting the impact of the crosstalk between PCD and cellular immunity on CRC prognosis. This reflects that the model Score, by comprehensively considering both cellular immunity and PCD, as well as their crosstalk, has achieved significant effectiveness in prognostic prediction.

The present study investigated the relationship between Score, immunotherapy response, and MSI. MSI has been reported to correlate with immunotherapy response in patients with CRC. In MSS-type CRC, only 5-20% of patients experience tumor regression following combination immunotherapy (20). However, ~50% of patients with MSI-H CRC also exhibit primary resistance to immunotherapy, particularly in metastatic cases (21). Due to the heterogeneity of CRC, MSI is not an ideal biomarker for predicting immunotherapy response. As a result, numerous research teams are actively seeking more promising biomarkers. In the present study, the proposed biomarker, Score, shows a strong association with

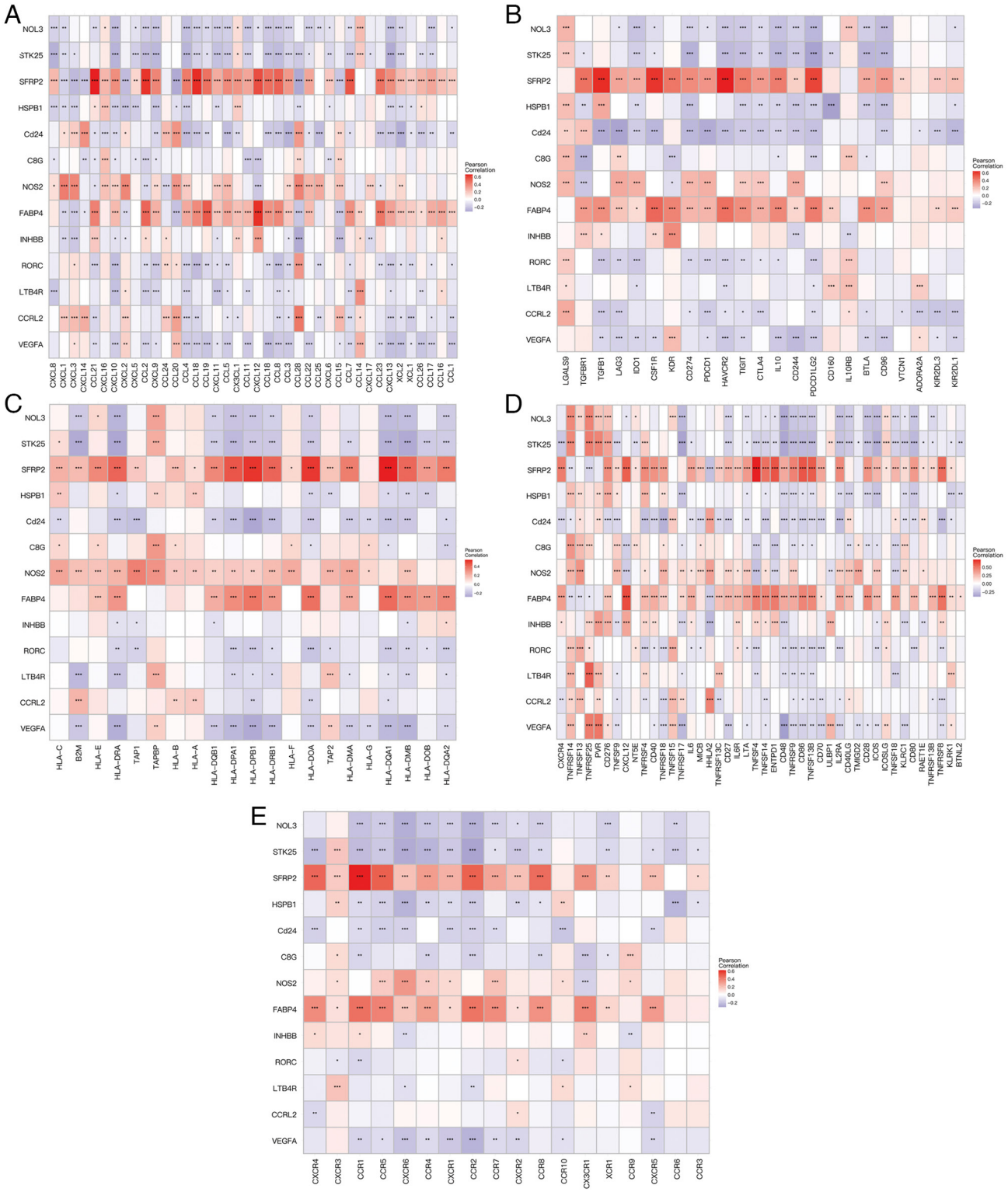

Figure 7. Association of 13 feature genes with immunity. (A) Correlation coefficient graph showing expression correlation between the 13 included genes and chemokine-related genes in the TCGA-COAD dataset. (B) Graph showing expression correlation between the 13 included genes and immune inhibitor genes in the TCGA-COAD dataset. (C) Graph showing expression correlation between the 13 included genes and major histocompatibility complex-related genes in the TCGA-COAD dataset. (D) Expression correlation between the 13 included genes and immune stimulation-related genes in the TCGA-COAD dataset. (E) Correlation coefficient graph of expression between the 13 included genes and receptor-related genes in the TCGA-COAD dataset. TCGA, The Cancer Genome Atlas; COAD, colon adenocarcinoma. *P<0.05; **P<0.01; ***P<0.001.

immunotherapy response in patients with CRC (Fig. 4M), but no significant correlation with microsatellite stability status (Fig. 4G), suggesting its potential as an MSI-independent predictor of immunotherapy response.

The present study further explored the relationship between Score and TME, as well as the response to immunotherapy. Immune cell infiltration was compared and it was found that the abundance of immune cells, including $CD4^{+}$ memory

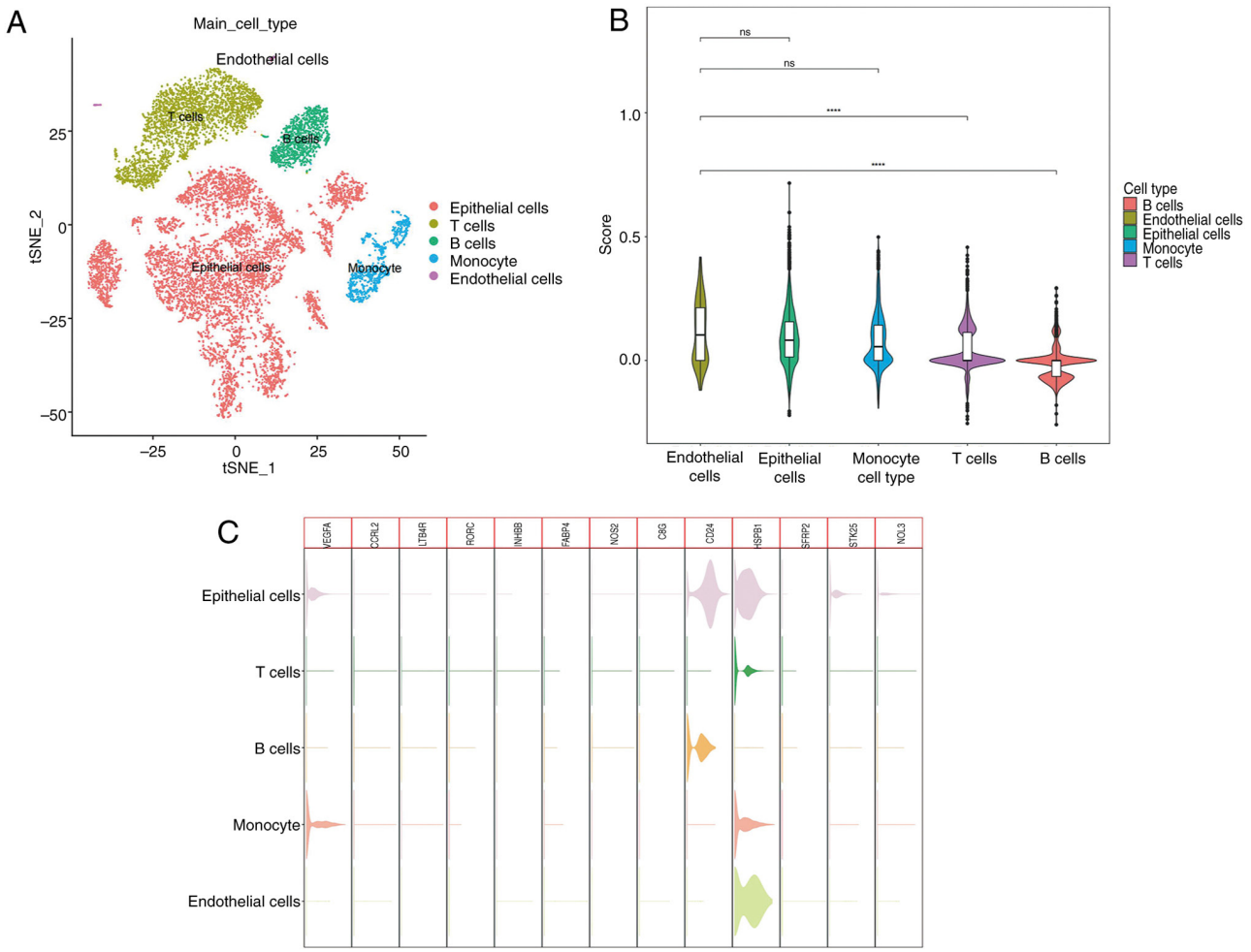

Figure 8. Single-cell analysis results. (A) t-SNE plot showing various cell types in the GSE161277 dataset. (B) Comparison of Score across different cell types. (C) t-SNE plot representing the expression levels of the 13 feature genes in various cell types. P<0.0001. t-SNE, t-distributed stochastic neighbor embedding; ns, no significance. ****P<0.0001.

T cells, $CD8^+$ naive T cells, $CD8^+$ T cells, $CD4^+$ T cells, $CD8^+$ memory T cells and NK cells, was higher in the low Score group (Fig. 4C). Correlation analysis revealed a negative relationship between the Score and the infiltration of 12 different immune cell types (Fig. 4D). Additionally, analysis of 29 Fges showed that the scores of antitumor immunity Fges were significantly higher in the low Score group compared with the high Score group (Fig. 4E). A significant difference in the proportions of immune phenotypes between the two groups was demonstrated in Fig. 4F. Furthermore, the scores of MDSCs, CAFs, TAM. M2 Exclusion and Dysfunction were notably higher in the high Score group compared with the low Score group (P<0.05; Fig. 4H-K). These findings suggested that the interaction between PCD and cellular immunity may affect prognosis by acting on TME. In the single-cell analysis of the GSE161277 dataset (Fig. 8B), it was observed that endothelial cells had the highest Score, while B cells had the lowest, suggesting that endothelial cells and B cells might be key carriers of the crosstalk between cellular immunity and PCD. Furthermore, TIDE score was significantly higher in the high Score group compared with the low Score group (Fig. 4L), indicating that the high Score group has a poorer response to ICI immunotherapy. There was no significant correlation between the Score and MSI (Fig. 4G), indicating that the Score serves as a signature for reflecting the degree of immunotherapy response and is not dependent on MSI. In the analysis of gene variations, an increase in mutations of genes such as TP53, SNX1 and ELAPOR1 was observed in the high score group. The mutation of the TP53 tumor suppressor gene is a clear driver of CRC development and is a poor prognostic factor for metastatic CRC (22). Additionally, TP53 gene mutations indicate a poor response to immunotherapy in patients (23). As tumor suppressors, mutations in SNX1 and ELAPOR1 can promote cell proliferation and invasion in CRC (24,25). In the low Score group, mutations in genes such as SCN5A increased. It has been reported that silencing SCN5A suppresses the cell cycle and EMT, reducing proliferation, migration and invasion, while enhancing apoptosis induced by 5-FU (26).

The present study also aimed to identify key genes that impact the prognosis of patients with CRC, focusing on 13 feature genes involved in the crosstalk between cellular immunity and PCD. Among these, LTB4R, VEGFA, FABP4, HSPB1 and SFRP2 are considered as risk factors in prognosis analysis, while RORC, NOS2, and other genes are recognized as significant protective factors. VEGFA, a member of the PDGF/VEGF growth factor family, promotes the proliferation and migration of vascular endothelial cells and plays a crucial role in both physiological and pathological angiogenesis. It has

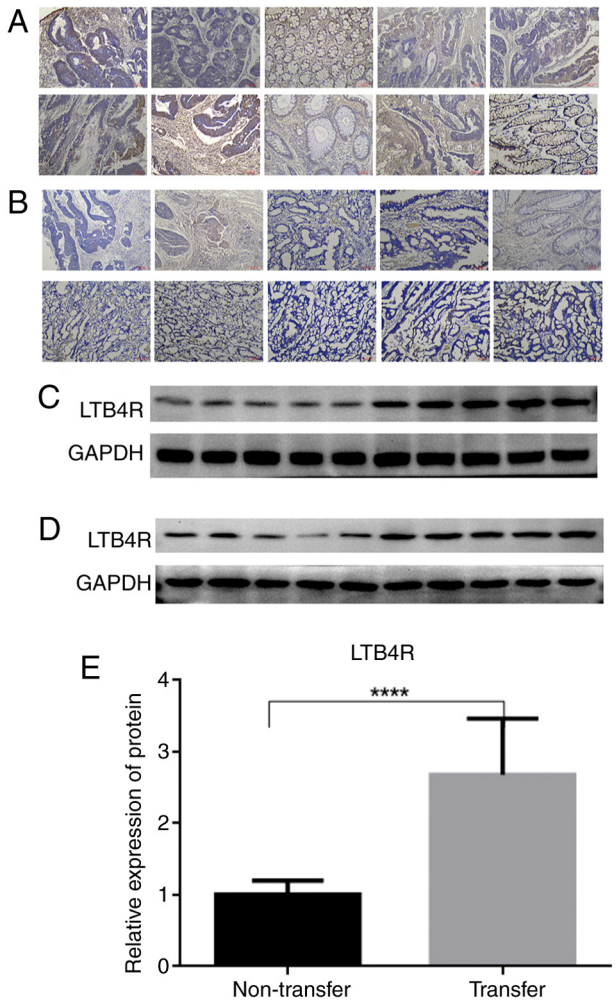

Figure 9. Analysis of LTB4R expression. (A) IHC results for LTB4R in colon cancer specimens from the transfer group. (B) IHC results for LTB4R in colon cancer specimens from the non-transfer group. (C) Western blot results showing LTB4R expression in colon cancer specimens of the transfer group. (D) Western blot results showing LTB4R expression in colon cancer specimens of the non-transfer group. (E) Comparison of LTB4R expression between the transfer and non-transfer groups based on western blot results. P<0.0001. IHC, immunohistochemical. ****P<0.0001.

been presviously indicated that VEGFA protein expression is significantly positively correlated with the infiltration of B cells and M2 macrophages, affecting CRC prognosis by influencing the abundance of B cells and macrophages in TME (27). FABP4 is related to tumor progression and poor prognosis across various cancers, with its low expression linked to the infiltration of B cells, $CD4^+$ T cells, $CD8^+$ T cells, myeloid dendritic cells, macrophages and neutrophils (28). The heat shock protein β-1 (HSPB1) gene encodes a protein involved in the differentiation of various cell types. Its expression is correlated with poor clinical outcomes in multiple human cancers, as its encoded protein may promote cancer cell proliferation and metastasis while protecting them from apoptosis. HSPB1 is also regarded as a negative regulator of ferroptosis in cancer cells. Protein kinase C-mediated HSPB1 phosphorylation reduces the production of iron-mediated lipid reactive oxygen species, thereby protecting cancer cells from ferroptosis (29). The gene signature composed of HSPB1 has been proven to reflect the TME and tumor immunity in liver cancer (30), colorectal adenocarcinoma (31) and glioma (32). Methylation of SFRP2 gene is a potential biomarker for CRC, and its upregulation can weaken WNT signaling in human colon cancer cell lines (33). Upregulating SFRP2 results in the weakness of WNT signal pathway transmission in human colon cancer cell lines (33). Multiple studies have revealed the interactions between tumor cells and the TME mediated by SFRP2 (34-36), highlighting the potential of SFRP2 as a prognostic biomarker (37,38). RORC and NOS2, as significant protective factors, are significantly downregulated in colon cancer tissues. Among them, RORC encodes a DNA-binding transcription factor and is a member of the nuclear hormone receptor NR1 subfamily. It has been revealed that RORC exhibits either high or low methylation in various cancers and is closely associated with immune cell infiltration and immunomodulators in these cancers (39). NOS2 produces low levels of nitric oxide in tumor cells, which significantly impacts tumor cell development (40,41). The spatial expression of NOS2 and COX2, as well as their interactions with T cells and macrophages, is currently a significant focus in TME and tumor immunity research. The present study also investigated the general expression correlation of these genes with chemokines, immune inhibitors, MHC-related genes, immune stimulation-related genes, and receptor-related genes. Additionally, these genes exhibit differential expression in tumor and paracancerous tissues of CRC. The present study further analyzed the driving factors behind abnormal expression of these feature genes, including gene mutations, methylation and CNVs.

The present study focuses on LTB4R, which is one of the feature genes involved in the crosstalk. The LTB4R gene encodes the leukotriene B4 receptor, which serves as a high-affinity receptor for leukotriene B4. The gene exerts various effects on different cell types, with the most notable being its chemotactic influence on neutrophils and macrophages (42). Previous studies have found that LTB4R is expressed in various cells in TME, including both immune cells (such as macrophages, activated T cells and dendritic cells) and non-immune cells (such as smooth muscle cells and endothelial cells) (43-45), highlighting its direct role in controlling adaptive immune responses. In analyzing the TCGA-COAD dataset, it was found that LTB4R expression was significantly upregulated in colon cancer tissues and is negatively correlated with the expression of most chemokines, immune inhibitors, MHC-related genes, immune stimulation-related genes and receptor-related genes. Although current research predominantly explores the association between LTB4R expression and tumor proliferation and development in animal models (46), clinical evidence remains insufficient. The present study further examines the relationship between LTB4R expression and CRC progression, revealing a significant positive correlation with cancer recurrence and metastasis. These findings suggest potential new targets for CRC treatment.

The present study explored the combined impact of cellular immunity and PCD on CRC prognosis and developed a machine learning model-based risk score combing both cellular immunity and PCD to accurately assess patient outcomes, facilitate risk stratification, and improve clinical management for patients with CRC. Subsequently, the research identified feature genes involved in the crosstalk between cellular immunity and PCD and provided an in-depth analysis of these

genes in terms of prognosis and tumor immunity, offering new tumor markers and therapeutic strategies for CRC. However, the present study has certain limitations, notably the need for further experimental validation of the specific roles of these 13 genes in the biological processes of CRC. Additionally, due to the relatively small sample size included in the biological experiments of the present study, the investigation into genes such as LTB4R was not conducted in depth. Subsequent studies will continue to investigate the biological effects of genes such as LTB4R and elucidate the mechanisms through which they influence the prognosis of CRC. Despite this, the research provides significant insights and potential value.

Acknowledgements

Not applicable.

Funding

No funding was received.

Availability of data and materials

The data generated in the present study may be requested from the corresponding author.

Authors' contributions

CW, SC, YH and QW conceived and designed the study; and critically revised the manuscript for important intellectual content. YC conceived and designed the study; acquired, analyzed and interpreted the data; and drafted the manuscript. CW and QW confirm the authenticity of all the raw data. All authors read and approved the final version of the manuscript.

Ethics approval and consent to participate

The present study was carried out in compliance with the Declaration of Helsinki and was approved (approval no. 2023-002-013) by the Institutional Review Committee of Zhanjiang Central People's Hospital (Zhanjiang, China). Written informed consent was provided by all participants.

Patient consent for publication

Not applicable.

Competing interests

The authors declare that they have no competing interests.

References

1. Lin Y, Pan X, Chen Z, Lin S, Shen Z and Chen S: Prognostic value and immune infiltration of novel signatures in colon cancer microenvironment. Cancer Cell Int 21: 679, 2021.
2. Wang Z, Liu Q, Chen Q, Zhu R and Zhu HG: Overexpression of NDRG1: Relationship with proliferative activity and invasiveness of breast cancer cell line and breast cancer metastasis. Zhonghua Bing Li Xue Za Zhi 35: 333-338, 2006 (In Chinese).
3. Pan B, Zheng B, Xing C and Liu J: Non-canonical programmed cell death in colon cancer. Cancers (Basel) 14: 3309, 2022.
4. Liu J, Hong M, Li Y, Chen D, Wu Y and Hu Y: Programmed cell death tunes tumor immunity. Front Immunol 13: 847345, 2022.
5. Wu L, Lu H, Pan Y, Liu C, Wang J, Chen B and Wang Y: The role of pyroptosis and its crosstalk with immune therapy in breast cancer. Front Immunol 13: 973935, 2022.
6. Bin Y, Ding P, Liu L, Tong F and Dong X: Classification of the immune microenvironment associated with 12 cell death modes and construction of a prognostic model for squamous cell lung cancer. J Cancer Res Clin Oncol 149: 9051-9070, 2023.
7. Zou Y, Xie J, Zheng S, Liu W, Tang Y, Tian W, Deng X, Wu L, Zhang Y, Wong CW, *et al*: Leveraging diverse cell-death patterns to predict the prognosis and drug sensitivity of triple-negative breast cancer patients after surgery. Int J Surg 107: 106936, 2022.
8. Zhou J, Yang S, Zhu D, Li H, Miao X, Gu M, Xu W, Zhang Y, Tang W, Shen R, *et al*: The crosstalk between anoikis and epithelial-mesenchymal transition and their synergistic roles in predicting prognosis in colon adenocarcinoma. Front Oncol 13: 1184215, 2023.
9. Chen L, Niu X, Qiao X, Liu S, Ma H, Shi X, He X and Zhong M: Characterization of interplay between autophagy and ferroptosis and their synergistical roles on manipulating immunological tumor microenvironment in squamous cell carcinomas. Front Immunol 12: 739039, 2022.
10. Liu Z, Liu L, Weng S, Guo C, Dang Q, Xu H, Wang L, Lu T, Zhang Y, Sun Z and Han X: Machine learning-based integration develops an immune-derived lncRNA signature for improving outcomes in colorectal cancer. Nat Commun 13: 816, 2022.
11. Bagaev A, Kotlov N, Nomie K, Svekolkin V, Gafurov A, Isaeva O, Osokin N, Kozlov I, Frenkel F, Gancharova O, *et al*: Conserved pan-cancer microenvironment subtypes predict response to immunotherapy. Cancer Cell 39: 845-865.e7, 2021.
12. Wang J, Gong R, Zhao C, Lei K, Sun X and Ren H: Human FOXP3 and tumour microenvironment. Immunology 168: 248-255, 2023.
13. Ke J, Wu X, Wu X, He X, Lian L, Zou Y, He X, Wang H, Luo Y, Wang L and Lan P: A subpopulation of $CD24^+$ cells in colon cancer cell lines possess stem cell characteristics. Neoplasma 59: 282-288, 2012.
14. Liu S, Liu C, Wang Y, Chen J, He Y, Hu K, Li T, Yang J, Peng J and Hao L: The role of programmed cell death in osteosarcoma: From pathogenesis to therapy. Cancer Med 13: e7303, 2024.
15. Gao L, Shay C and Teng Y: Cell death shapes cancer immunity: Spotlighting PANoptosis. J Exp Clin Cancer Res 43: 168, 2024.
16. Fedele P, Santoro AN, Pini F, Pellegrino M, Polito G, De Luca MC, Pignatelli A, Tancredi M, Lagattolla V, Anglani A, *et al*: Immunonutrition, metabolism, and programmed cell death in lung cancer: Translating bench to bedside. Biology (Basel) 13: 409, 2024.
17. Wu X, Cao J, Wan X and Du S: Programmed cell death in hepatocellular carcinoma: Mechanisms and therapeutic prospects. Cell Death Discov 10: 356, 2024.
18. Baldi S, He Y, Ivanov I, Sun Y, Feng W, Refat M, Mohammed SAD, Adlat S, Tian Z, Wang Y, *et al*: Novel characterization discoveries of ferroptosis-associated molecules in COAD microenvironment based TCGA data. Front Mol Biosci 9: 1102735, 2022.
19. Nagata S and Tanaka M: Programmed cell death and the immune system. Nat Rev Immunol 17: 333-340, 2017.
20. Fukuoka S, Hara H, Takahashi N, Kojima T, Kawazoe A, Asayama M, Yoshii T, Kotani D, Tamura H, Mikamoto Y, *et al*: Regorafenib plus nivolumab in patients with advanced gastric or colorectal cancer: An Open-label, dose-escalation, and Dose-expansion phase Ib trial (REGONIVO, EPOC1603). J Clin Oncol 38: 2053-2061, 2020.
21. Diaz LA Jr, Shiu KK, Kim TW, Jensen BV, Jensen LH, Punt C, Smith D, Garcia-Carbonero R, Benavides M, Gibbs P, *et al*: Pembrolizumab versus chemotherapy for microsatellite instability-high or mismatch repair-deficient metastatic colorectal cancer (KEYNOTE-177): Final analysis of a randomised, open-label, phase 3 study. Lancet Oncol 23: 659-670, 2022.
22. Wakayama S, Ouchi K, Takahashi S, Yamada Y, Komatsu Y, Shimada K, Yamaguchi T, Shirota H, Takahashi M and Ishioka C: TP53 Gain-of-Function mutation is a poor prognostic factor in High-methylated metastatic colorectal cancer. Clin Colorectal Cancer 22: 327-338, 2023.
23. Kim JY, Jung J, Kim KM, Lee J and Im YH: TP53 mutations predict poor response to immunotherapy in patients with metastatic solid tumors. Cancer Med 12: 12438-12451, 2023.
24. Bian Z, Feng Y, Xue Y, Hu Y, Wang Q, Zhou L, Liu Z, Zhang J, Yin Y, Gu B and Huang Z: Down-regulation of SNX1 predicts poor prognosis and contributes to drug resistance in colorectal cancer. Tumour Biol 37: 6619-6625, 2016.

25. Huang A, Qin C, Wu M, Zhang D, Wu G and Sun P: ELAPOR1 suppresses tumor progression in colorectal cancer and indicates favorable prognosis. Cancer Biomark 37: 279-288, 2023.
26. Sui Q, Peng J, Han K, Lin J, Zhang R, Ou Q, Qin J, Deng Y, Zhou W, Kong L, *et al*: Voltage-gated sodium channel Nav1.5 promotes tumor progression and enhances chemosensitivity to 5-fluorouracil in colorectal cancer. Cancer Lett 500: 119-131, 2021.
27. Zhuang Z, Cai H, Lin H, Guan B, Wu Y, Zhang Y, Liu X, Zhuang J and Guan G: Development and validation of a robust Pyroptosis-related signature for predicting prognosis and immune status in patients with colon cancer. J Oncol 2021: 5818512, 2021.
28. Wu D, Xiang L, Peng L, Gu H, Tang Y, Luo H, Liu H and Wang Y: Comprehensive analysis of the immune implication of FABP4 in colon adenocarcinoma. PLoS One 17: e0276430, 2022.
29. Quail DF and Joyce JA: Microenvironmental regulation of tumor progression and metastasis. Nat Med 19: 1423-1437, 2013.
30. Lin S, Li D, Yang Y, Yu M, Zhao R, Li J and Peng L: Single-cell RNA-seq elucidates the crosstalk between cancer stem cells and the tumor microenvironment in hepatocellular carcinoma. J Cancer 15: 1093-1109, 2024.
31. Yang G, Wang H and Sun B: Construction of cuproptosis-associated prognostic signature in colon adenocarcinoma based on bioinformatics and RT-qPCR analysis. Oncol Lett 25: 91, 2023.
32. Chen L and Fu B: T cell exhaustion assessment algorism in tumor microenvironment predicted clinical outcomes and immunotherapy effects in glioma. Front Genet 13: 1087434, 2022.
33. Zhang Y and Chen H: Genistein attenuates WNT signaling by up-regulating sFRP2 in a human colon cancer cell line. Exp Biol Med (Maywood) 236: 714-722, 2011.
34. Charles Jacob HK, Signorelli R, Charles Richard JL, Kashuv T, Lavania S, Middleton A, Gomez BA, Ferrantella A, Amirian H, Tao J, *et al*: Identification of novel early pancreatic cancer biomarkers KIF5B and SFRP2 from 'first contact' interactions in the tumor microenvironment. J Exp Clin Cancer Res 41: 258, 2022.
35. Mo S, Shen X, Wang Y, Liu Y, Sugasawa T, Yang Z, Gu W and Nakajima T: Systematic single-cell dissecting reveals heterogeneous oncofetal reprogramming in the tumor microenvironment of gastric cancer. Hum Cell 36: 689-701, 2023.
36. Croft W, Pearce H, Margielewska-Davies S, Lim L, Nicol SM, Zayou F, Blakeway D, Marcon F, Powell-Brett S, Mahon B, *et al*: Spatial determination and prognostic impact of the fibroblast transcriptome in pancreatic ductal adenocarcinoma. Elife 12: e86125, 2023.
37. Yang Z, Zhou D and Huang J: Identifying explainable machine learning models and a novel SFRP2+ fibroblast signature as predictors for precision medicine in ovarian cancer. Int J Mol Sci 24: 16942, 2023.
38. Lautert-Dutra W, Melo CM, Chaves LP, Souza FC, Crozier C, Sundby AE, Woroszchuk E, Saggioro FP, Avante FS, Dos Reis RB, *et al*: Identification of tumor-agnostic biomarkers for predicting prostate cancer progression and biochemical recurrence. Front Oncol 13: 1280943, 2023.
39. He S, Yu J, Sun W, Sun Y, Tang M, Meng B, Liu Y and Li J: A comprehensive pancancer analysis reveals the potential value of RAR-related orphan receptor C (RORC) for cancer immunotherapy. Front Genet 13: 969476, 2022.
40. Castro ED, Mathias PPM, Batista WL, Sato AYS, Toledo MS, de Almeida VT, Curcio MF, da Costa PE, Stern A and Monteiro HP: Knockdown of the inducible nitric oxide synthase (NOS2) splicing variant S3 promotes autophagic cell death from nitrosative stress in SW480 human colon cancer cells. Cell Biol Int 46: 158-169, 2022.
41. Ambs S, Merriam WG, Bennett WP, Felley-Bosco E, Ogunfusika MO, Oser SM, Klein S, Shields PG, Billiar TR and Harris CC: Frequent nitric oxide synthase-2 expression in human colon adenomas: Implication for tumor angiogenesis and colon cancer progression. Cancer Res 58: 334-341, 1998.
42. Yokomizo T, Izumi T, Chang K, Takuwa Y and Shimizu T: A G-protein-coupled receptor for leukotriene B4 that mediates chemotaxis. Nature 387: 620-624, 1997.
43. Bäck M, Bu DX, Bränström R, Sheikine Y, Yan ZQ and Hansson GK: Leukotriene B4 signaling through NF-kappaB-dependent BLT1 receptors on vascular smooth muscle cells in atherosclerosis and intimal hyperplasia. Proc Natl Acad Sci USA 102: 17501-17506, 2005.
44. Goodarzi K, Goodarzi M, Tager AM, Luster AD and von Andrian UH: Leukotriene B4 and BLT1 control cytotoxic effector T cell recruitment to inflamed tissues. Nat Immunol 4: 965-973, 2003.
45. Del Prete A, Shao WH, Mitola S, Santoro G, Sozzani S and Haribabu B: Regulation of dendritic cell migration and adaptive immune response by leukotriene B4 receptors: A role for LTB4 in up-regulation of CCR7 expression and function. Blood 109: 626-631, 2007.
46. Long S, Ji S, Xiao K, Xue P and Zhu S: Prognostic and immunological value of LTB4R in pan-cancer. Math Biosci Eng 18: 9336-9356, 2021.